International Journal of Coal Science & Technology (2023) 10:20
https://doi.org/10.1007/s40789-023-00578-5

RESEARCH

Effects of coals microscale structural features on their mechanical properties, propensity to crushing and fine dust formation

Elena Kossovich[1] · Svetlana Epshtein[1] · Vera Krasilova[1] · Jie Hao[1] · Maxim Minin[1]

Received: 22 March 2022 / Revised: 27 June 2022 / Accepted: 1 March 2023

Abstract
The work is dedicated to revealing the structural features of coals with different ranks, such as anthracites, metaanthracite and graphite, that determine their ability to crush and form fine dust. For this purpose, a combination of various nanoindentation techniques and Raman spectroscopy was used. The mechanical behavior of the selected coals was investigated by cyclic nanoindentation with increasing peak load and quasi-static loading. The alteration of the mechanical properties was studied by analysis of elastic moduli and damage indices R_w. Three groups of coals were identified based on their propensity to crushing during cyclic nanoindentation. Coals assigned to the first and second groups are characterized by local destruction in the contact zone with the indenter and the formation of a core of crushed material. Coals assigned to the third group are characterized by bulk destruction (outside the zone of contact with the indenter). In general, the ability of coals to fracture under mechanical loading decreases in the series of metamorphism due to microscale compaction of vitrinite matter. In the series of anthracite, metaanthracite and graphite, it is established that the coal matter compaction takes place for the anthracite and metaanthracite, whereas graphite reveals rather different behavior due to abrupt change of its structure. The ratios between the amorphous and crystalline phases of carbon (S) were determined by deconvolution of coals Raman spectra. The propensity of coals to crushing (a damage index R_w) increases with growth of the proportion of amorphous carbon in the coal matter. For the considered coals and metaanthracite, it is established that the proneness to destruction outside the contact zone with the indenter is determined by the ratio of amorphous and crystalline carbon of 1 and higher. When S parameter is lower than 1, the coals are being crushed only in the zone of contact with the indenter.

Keywords Coal · Crushing · Cyclic nanoindentation · Raman spectroscopy · Amorphous carbon · Crystalline carbon

1 Introduction

Coal dust formation and emission is a naturally accompanying process for ones of mining, storage, transportation and transshipment of coals. During all the coals' lifecycle, dust emission endangers the workers' health (Erol et al. 2013; Liu and Liu 2020; Shekarian et al. 2021) as well as the environmental safety (e.g. by air flows-based migration of fine coal dust bearing concentrates of potentially toxic elements to soil and underground and overground waters (Aneja et al. 2012; Pandey et al. 2016; Moreno et al. 2019). Also it is worth mentioning that coals' crushing during transportation leads not only to dust formation and emission, but also to the losses in supply chain due to crushing to finer classes (Baruya 2012).

The current researches on studying the coal dust formation mechanism are based on an assumption that the latter is being produced and released under mechanical impacts during the seam opening and cutting, also at transportation and transshipment of products (Luo et al. 2017). In the middle of the XX century, some experimental relations were found between the amount of the released dust and coal rank (Beron et al. 1971). The latter was also studied by using the mathematical modeling based on fracture mechanics approaches (Panov 1967). Most of the experiments were based on Hargrove grindability index evaluation along with size analysis of the particles formed (Baafi and Ramani 1979; Hower et al. 1987). This allowed establishing the positive correlation between coals rank and the amount of fine

✉ Elena Kossovich
e.kossovich@misis.ru

[1] National University of Science and Technology "MISIS", 4, build.1, Leninsky prospect, Moscow 119049, Russian Federation

dust (less than ~60 μm) and no correlation with the maceral composition of (Baafi and Ramani 1979; Organiscak and Page 1993, 2000). Although, the latest research revealed that high inertinite contents could be one of the reasons of relatively high amount of fine (less than 10 μm) coal dust formation and release into the air (Epshtein et al. 2020).

Current perceptions on interconnections between coals' mechanical properties and their propensity to fine aerosol dust formation after the external impacts are based primarily on the fact that structural defects formation is predominantly occurs at micro- and nanoscales. Consequently, it is easy to assume that the mechanical properties that determine coals propensity to dust formation, should be characterized at the corresponding scales (Zhang et al. 2018; Si et al. 2020; Fender et al. 2020). It was shown that micro- and nanoindentation of coals (as brittle materials) leads to their destruction with the formation of a core of crushed material (Argatov et al. 2017; Zhou et al. 2019). Recent works also allowed revealing that coals propensity to crushing under mechanical impacts is primarily determined by homogeneity or heterogeneity of their vitrinites. This was assumed during investigation of vitrinite-rich bituminous coals originating from the same seam but from packs that are different in potential proneness to sudden outbursts of dust and gas (Epshtein et al. 2018; Ul'yanova et al. 2019). Later, a mathematical model was proposed that allows evaluation of the sizes of particles formed during indentation on the basis of data on the micro- and macro-mechanical characteristics of coals (Kossovich et al. 2020a). It was found that the sizes of the particles formed after indentation experiments differ significantly for coals of different rank. This, presumably, is associated with the features of the supramolecular structure of the organic matter of coals (see, e.g., Hirsch 1954; Epshtein et al. 2007). Therefore, the information on the coals structural characteristics is important in terms of achieving their propensity to crushing with dust formation. One of the most efficient means for retrieving such data is Raman spectroscopy. Recent studies allowed for the semi-quantification of some inner structural characteristics of coals organic matter and their variation with rank and genetic and metamorphism conditions (Ulyanova et al. 2014; Han et al. 2017; Xu et al. 2018; Huan et al. 2019; Vasilenko et al. 2020).

The aim of the current paper is to reveal the structural features of hard coals of different ranks, anthracites, metaanthracite and graphite, that determine their ability to crushing with fine dust formation during these processes. To this end, a combination of different nanoindentation techniques was used with Raman spectroscopy for characterization of the differences between structures of all the considered coals vitrinites.

2 Materials and methods

2.1 Objects of study

The objects of study included bituminous coals of different rank, origin, and petrographic composition (6 items), two anthracites varying in their origin and rank, metaanthracite and graphite. Some main characteristics of these coals are listed in Table 1.

Bituminous coals from the Kuznetsk basin (No. 1, 4, 5, 6) vary in rank. Coal No. 5 has the highest contents of inertinite (51.8% vol.) among all the selected coals.

The Pechora basin coals (No. 2, 3) were extracted from the same seam but from packs that differ in their proneness to sudden outbursts of coal and gas.

Anthracite No. 7, metaanthracite No. 8 and graphite No. 10 are originating from the same deposit but extracted from different packs with varying conditions of the contact and thermal metamorphism (Kossovich et al. 2020b).

Samples (polished sections) were prepared in accordance with a previously developed technique (Kossovich et

Table 1 Characteristics of coals samples used in the research

No. of the sample	Type	Origin	Vitrinite reflectance $R_{o,r}$ (%vol)	Maceral composition (%vol)		
				Vitrinite Vt	Inertinite I	Liptinite L
1	Bituminous coal	Kuznetsk basin	0.65	70.0	20.0	10.0
2	Bituminous coal	Pechora basin	0.89	91.0	7.0	2.0
3	Bituminous coal	Pechora basin, pack potentially prone to sudden outbursts	0.92	86.0	13.0	1.0
4	Bituminous coal	Kuznetsk basin	0.95	56.4	41.6	2.0
5	Bituminous coal	Kuznetsk basin	1.13	47.6	51.8	0.6
6	Bituminous coal	Kuznetsk basin	1.65	66.5	33.5	0
7	Anthracite	Omsukchansk coalfield	2.57	-	-	-
8	Metaanthracite	Omsukchansk coalfield	3.28	-	-	-
9	Anthracite	Donetsk basin	3.58	91.0	9.0	0
10	Graphite	Omsukchansk coalfield	5.55	-	-	-

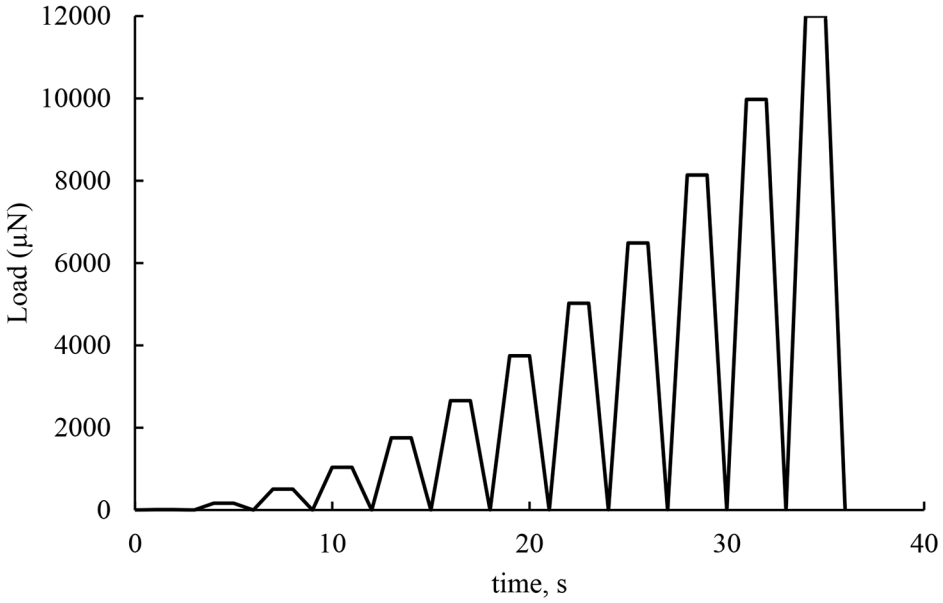

(a)

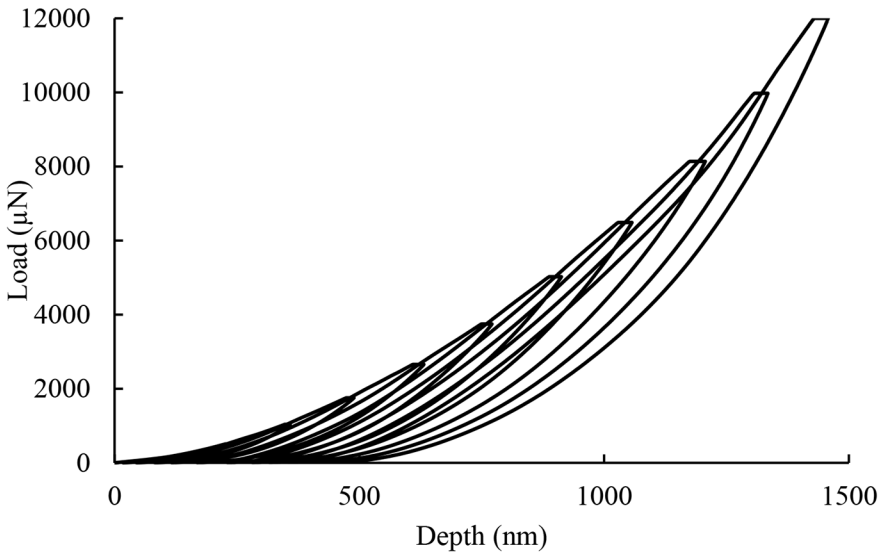

(b)

Fig. 1 **a** Loading mode for the cyclic nanoindentation **b** Example of *P-h* curve for cyclic nanoindentation (coal No. 2)

al. 2016) so that the surface prepared for indentation and Raman spectroscopy experiments was oriented perpendicular to the direction of bedding. Tests were carried out on vitrinite as on maceral, which is the most susceptible to changes in mechanical properties in the metamorphism series (Kossovich et al. 2016).

2.2 Nanoindentation experiments

In order to investigate the mechanical properties of coals and graphite, as well as their proneness to crushing, the classical nanoindentation technique was used along with the cyclic one.

For experiments on classical "single" and cyclic nanoindentation, Hysitron TI 750 UBI nanotriboindenter with a built-in surface analyzer (scanning probe microscopy) and TriboScan software for automated experimentation and data processing was used.

Experiments were held on the surface of a coal sample vitrinite. The surface must be characterized by optical uniformity, the absence of a pronounced relief (the roughness determined by scanning probe microscopy should not exceed 0.5 μm) and lack of various types of defects (cracks).

Classical "single" (i.e. quasi-static) nanoindentation experiments were carried out on selected sites (at least two for each of the coals) by grid indentation, where the grid nodes are the points of contact with the indenter. In total, at least 36 indentations were carried out on each of the sites. The value of the maximum load was selected individually for each of the coals. A trapezoidal protocol was used as a loading scheme: 5 s loading to the maximum value, 2 s exposure under maximum load, 5 s unloading (at a speed corresponding to the loading speed).

To assess the change in the mechanical properties of coals in the metamorphism series, the following data were measured and averaged over experiments on each of the coals:

(1) The value of the contact modulus of elasticity E, determined in accordance with the Bulychev-Alekhin-Shorshorov dependence (Bulychev et al. 1975) by the slope of the initial part of the unloading branch;
(2) Damage index, R_w. It characterizes the ability of a brittle material to fracture. Its choice is due to the fact that it was previously established that coals are a brittle material that can be crushed under low loading values (during nanoindentation) (Argatov et al. 2017). The damage index is determined based on the ratio of the hysteresis loop area of the loading-unloading curve, which is being built automatically by the nanohardness equipment, to the total work of the forces on loading the sample (Kossovich et al. 2020b).

Hardness, as a result of nanoindentation, was excluded from the results, since it was shown that this value is not a mechanical characteristic of coals due to their crushing during nanoindentation (Argatov et al. 2017).

For cyclic nanoindentation of coals vitrinites, we used the approach developed earlier (Kossovich et al. 2021) as a method for assessing the propensity of coals to destruction with the formation of dust. A twelve-stage cyclic loading mode was chosen, with the maximum loading value increasing exponentially from 0.01 to 12.00 mN and holding under the maximal load for 5 s. Thus, each loading cycle consisted of loading from 0 to the maximum (for a particular cycle) for 5 s, holding under peak load for 2 s, and unloading to zero also for five seconds. The graphic representation of the loading mode is shown in Fig. 1a. The cycles numbers and the corresponding peak load are given in Table 2. An example of the *P-h* curve plotted on the basis of such loading type is given in Fig. 2b (for coal No. 2).

Table 2 Assignment of cycles number and peak load P_{max}

Cycle No.	P_{max} (μN)
1	10
2	170
3	500
4	1000
5	1700
6	2600
7	3700
8	5000
9	6400
10	8100
11	10,000
12	12,000

According to the proposed method, for each of the loading cycles, the above-described indicators of the contact modulus of elasticity and the damage index were determined. For each sample, a set of data was obtained on the values of the modulus of elasticity and the damage index for eight separate cyclic loadings (each with twelve cycles). The data were averaged separately for each of the cycles, and the standard deviation of the values was also calculated (it did not exceed 5% of the average for both the elastic moduli and the damage indices).

Next, the dependences of the values of the modulus of elasticity and the damage index on the number of loading cycles were built.

2.3 Raman spectroscopy

Raman spectroscopy measurements were carried out to investigate the structural features of the selected samples. To this end, EnSpectr R532 Raman spectrometer mounted on Olympus BX 300 microscope was used. The spectrometer is operating with a universal green 532 nm lazer with resolution of 4 cm^{-1}. The laser power was set up to 5mW (depending on the property of the sample under study), integration time was 2 s. Measurements were performed at the samples' (polished sections) surface occupied with optically homogenous vitrinite in air at a room temperature. Not less than 30 measurements (each at different zone occupied by vitrinite) were performed at each sample. Further, the spectral data for each of the coal was averaged (by Raman ToolSet software) and processed to obtain the average smooth spectra in the range of Raman shift of 1000–1800 cm^{-1}.

Raman spectrometry results were then analyzed in accordance with the following scheme. Baseline subtraction was performed in order to eliminate the fluorescence effects. All the spectra were primarily characterized by two wide bands, called the "D" (~1360 cm^{-1}) and "G" (~1590 cm^{-1}). They are being found present for all the coals (Ulyanova et al. 2014; Xu et al. 2015; Nikitin et al. 2019). Commonly, the "G" band is associated with graphitic structures in coals, whereas the "D" one is being interpreted in various ways and most of the authors agree that it is a composition of a number of smaller separate bands associated with amorphous and disordered graphitic structures.

Table 3 Characteristics of the peaks for fitting the coals Raman spectroscopy data (for more details see (Sadezky et al. 2005; Ulyanova et al. 2014; Manoj 2016; Xu et al. 2018))

Name of the peak	Approximate position (1/cm) (Raman shift)	Characteristics	Carbon compounds type
SL	1230	Volatile hydrocarbon compounds, polyenes	Amorphous
D	1370	Graphite lattice defects, graphite edge defects	Crystalline
VR	1380	Methyl groups	Amorphous
VL	1460	Methylene groups	Amorphous
GR	1540	Amorphous carbon, aromatics with less than 5 rings	Amorphous
G	1580	Perfect graphitic structures	Crystalline
G2	1600	Disordered graphitic structures, surface graphitic layers	Crystalline

The exact positions (X D, X G,), intensity (I D, I G), areas (A D, A G) and full-width half-maximum (FWHM D, FWHM G) were evaluated for the aforementioned wide bands using peak fitting software with Gaussian type of peaks. The fitting tolerance was exceeding 97% which is rather low and reasoned by the asymmetry of these bands.

The asymmetry of the wide "D" and "G" bands, according to the reports of many authors, is primarily reasoned by the fact that they are the combination of smaller vibration bands in finer structures, including the crystalline and amorphous carbon compounds (Sadezky et al. 2005; Ulyanova et al. 2014; Xu et al. 2015, 2018; Manoj 2016; Jiang et al. 2021). Therefore, it is useful to analyze these wide bands by curve-fitting techniques in accordance with some model allowing attributing the modes of fitting to some fine structures that are found in coals. First model of such fitting was proposed by (Sadezky et al. 2005) and further expanded by many other authors (see their applications in, e.g. (Ulyanova et al. 2014; Manoj 2016; Xu et al. 2018)).

The model of peaks fitting used in this work well correlates with the ones previously discussed in (Sadezky et al. 2005; Ulyanova et al. 2014; Xu et al. 2018). It consists of seven locations fitted by the Lorentzian-type peaks. The characteristics of those structures are listed in Table 3. Their attribution to the fine structures (including crystalline and amorphous carbon compounds) is based on the aforementioned deconvolution models.

The decomposition of the coals spectral characteristics into such groups allowed confirming the 'amorphous-crystalline' peaks division due to vanishing of SL, VR, VL and GR peaks for the natural graphite (Li et al. 2021). It should be also noticed that for coals of different ranks, including anthracites and graphite, some of the peaks appear or disappear, presumably, due to evolution of their structure with rank.

Figure 2 demonstrates an example of curve fitting of the Raman spectra for coal No. 9. In all cases, the fitting tolerance exceeded 98.9%.

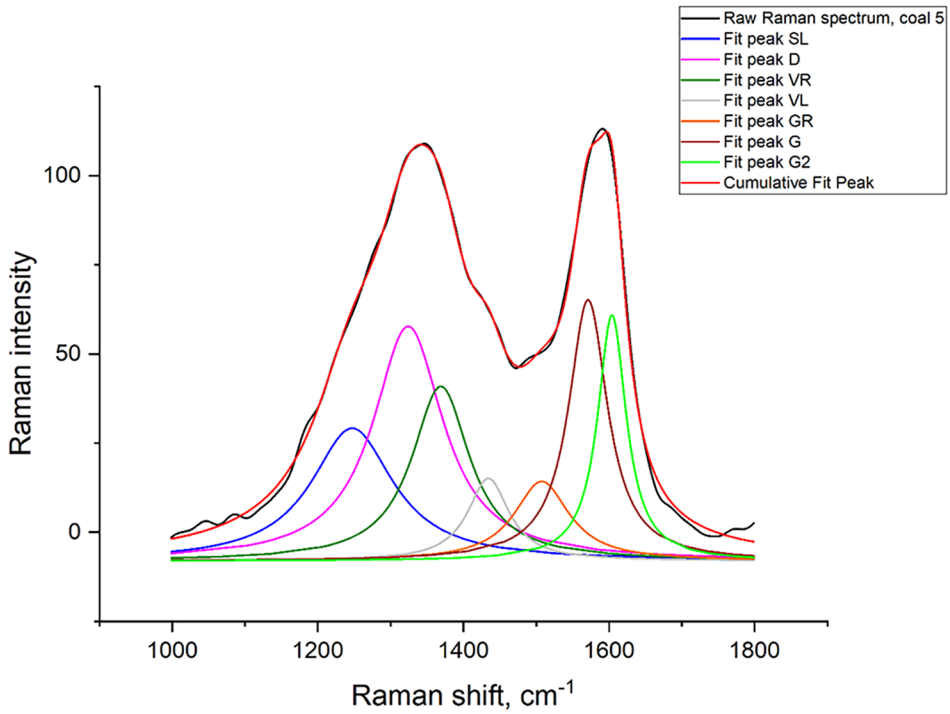

Fig. 2 Example of peaks fitting of the Raman spectral data (for coal No. 5)

3 Results and discussion

3.1 Mechanical properties and crushing of coals at microscale

Figure 3 shows the dependences of the change in the values of the damage index and the modulus of elasticity during cyclic nanoindentation.

Analysis of the results of cyclic nanoindentation of coals vitrinites allowed revealing three groups of coals with respect to the trends of elastic moduli and damage indices alteration from cycle to cycle.

The first (and most numerous) group included bituminous coals No. 1 and 5 of the Kuznetsk basin, No. 2 of the Pechora coal basin (the one from the non-hazardous pack), and highly-metamorphous anthracite No. 9. The reflectance of vitrinite for these coals varies within 0.65%–3.58%.

For this group of coals, the damage index gradually decreases with an increase in the number of cycles (and the magnitude of the applied load, respectively), the degree of its relative decay reaches up to 40% of the initial values. On the contrary, the value of the elastic modulus gradually increases up to approximately sixth or eighth loading cycle, after which it does not change significantly. Altogether, this indicates on high degree of compaction of coals matter during cyclic indentation reasoned presumably by crushing at the previous cycles and pressing (compaction) of the already formed powder at further cycles. Also, this demonstrates the local destruction of coals matter (i.e. in the contact zone with the indenter).

The second group included anthracite and metaanthracite of Omsukchansk coalfield (No. 7 and 8).

The damage index for coals of this group generally decreases for all loading cycles. The degree of its reduction is lower than for the first group and reaches 15% of the initial values. The modulus of elasticity increases linearly with the number of cyclic loads applied to the samples. Note that the mechanism of destruction of coals assigned to the first and second groups is generally close. The difference lies, apparently, in the amount and degree of compaction of the dust formed during the destruction. For coals of the second group, the amount of dust generated is not sufficient to prevent further destruction after its compaction. The

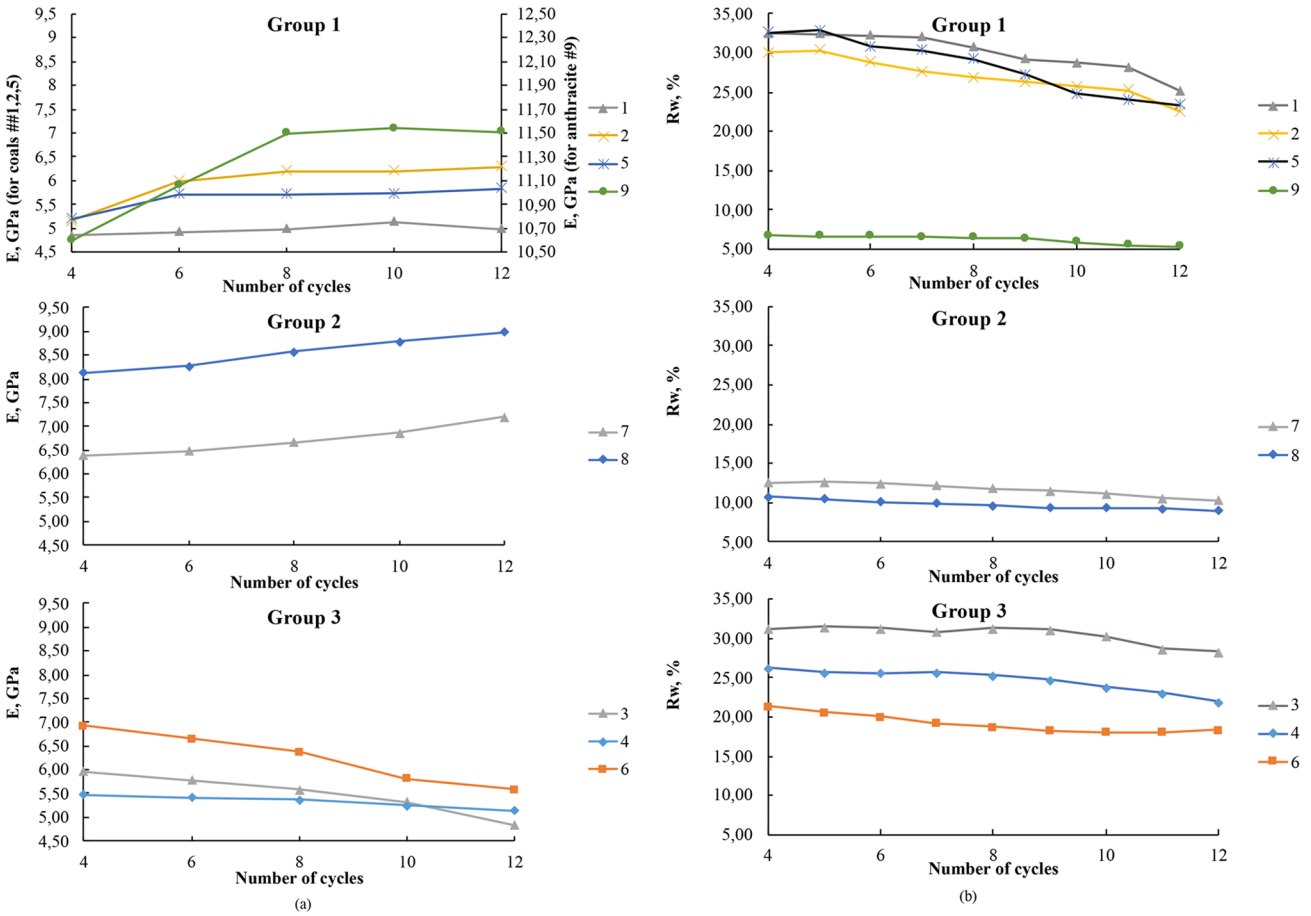

Fig. 3 Changes in **a** Elastic moduli and **b** Damage index for coals at cyclic nanoindentation: a division into groups

destruction of coals matter occurs also primarily in the contact zone with the indenter.

The third group of coals included samples of coal No. 3 of the Pechora basin (with vitrinite reflectance of 0.92% vol.) and No. 4 and 6 of the Kuznetsk basin with a vitrinite reflectance of 0.95% and 1.65% vol. These coals are characterized by an inversed (with respect to groups 1 and 2) pattern of changing in elastic moduli and damage indices with cycles number growth.

The damage index with an increase in the number of cycles changes least pronouncedly among all the considered groups of coals. The degree of its reduction from the initial values on average did not exceed 10%–15%. Also, there is a proportional decrease in the values of stiffness (modulus of elasticity) with the number of loading cycles. Altogether, this indicates on the bulk destruction of coals matter during cyclic nanoindentation without compaction of previously formed powder of dust particles. The bulk destruction of coals of the third group has been visualized by means of scanning probe microphotographs taken before and after the experiments (Fig. 4).

Behavior of graphite No. 10 during the cyclic nanoindentation has been discussed elsewhere and was characterized by both increase of the elastic moduli values and damage indices, and was assigned to a structure highly prone to destruction (Kossovich et al. 2021). Differences in the mode of destruction of graphite under cyclic loading from the above groups of coals can be explained by the fact that the structure of graphite is different from coals, less densely packed and mobile, which leads to "slippage" of individual layers and their blocks under the indenter, as shown in (Barsoum et al. 2004).

The division of the studied coals into groups, each of which includes coals from different deposits and the vitrinite reflectance index, suggests that there is no obvious dependence of the character of destruction and dust formation on the stage of metamorphism and even the origin of coals. Therefore, it can be assumed that the nature of the destruction of coals and the formation of dust under mechanical influences depends primarily on the structural features of the vitrinite substance.

Table 4 represents coals mechanical properties measured by the quasi-static and cyclic nanoindentation techniques.

The correlations between coals rank (with the exception of graphite) and their stiffness (or elastic moduli as the measure of this characteristic) are shown in Fig. 5 for both the quasi-static values (E) and those measured during nanoindentation at the tenth cycle (E_{10}).

It could be seen in Fig. 5 that both E and E_{10} increase with rank for anthracites and metaanthracite. Along with it, there could be observed almost no dependence of these values on rank for other coals. Also, for this range, the values of E and E_{10} are rather similar, whereas for higher-rank coals (with vitrinite reflectance over 2% vol.), elastic moduli measured at cyclic nanoindentation at the tenth cycle, are relatively higher than those measured by the quasi-static technique.

The relations between the damage indices measured during quasi-static nanoindentation (R_w) and after the tenth cycle (R_{w10}) with the coals vitrinite reflectance are given in Fig. 6. Note the decrease of both the considered damage indices with vitrinite reflectance index growth is observed for the whole range of the considered coals (excluding graphite), but values R_w are higher than those of R_{w10}. The latter also presumably indicates on the compaction of fine dust particles that were formed during previous cycles of nanoindentation (Kossovich et al. 2021).

The decay of the damage indices with coals' rank presumably indicate on the compaction of their structure and increase of their resistivity to external mechanical effects. These observations are in the frameworks of the previously obtained results (Vranjes et al. 2018; Zhang et al. 2020). The mechanisms of such alterations should be investigated using information on coals' fine structure characterized by Raman spectroscopy.

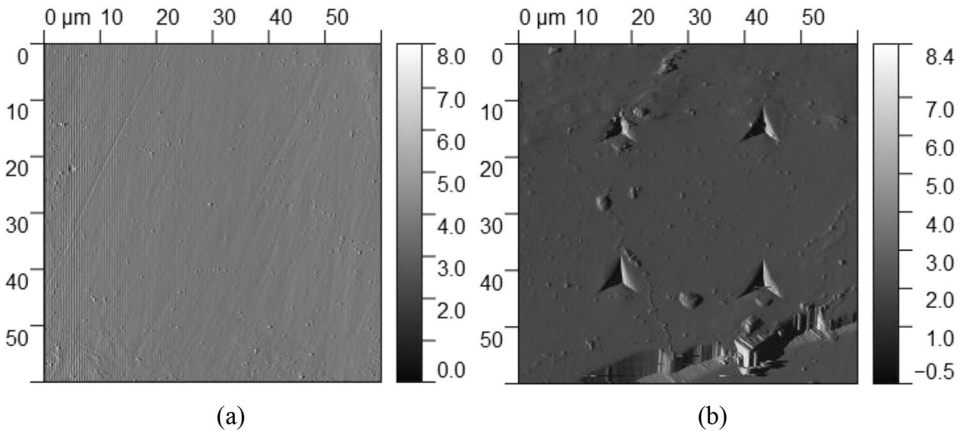

Fig. 4 An example of the image of the surface topology of coals **a** Before and **b** After cyclic nanoindentation. After mechanical impacts, a pronounced change (imprints, cracks outside the indentation zone, as well as destruction near the imprints are visible; pieces of a detached coal substance are found)

Table 4 Results of coals mechanical properties measurements at microscale

Sample No.	$R_{o,r}$ (%vol)	Quasi-static nanoindentation					Cyclic nanoindentation			
		P_{max} (μN)	E (GPa)	StDev E (GPa)	R_w (%)	StDev R_w (%)	E_{10} (GPa)	StDev E_{10} (GPa)	R_{w10} (%)	StDev R_{w10} (%)
1	0,65	4000	4,61	0,08	33,48	1.11	5.14	0.01	28.78	1.56
2	0,89	4000	6,48	0,18	39,65	2.03	6.20	0.06	25.70	2.44
3	0,92	4000	5,96	0,22	40,66	5.33	5.57	0.10	30.34	4.12
4	0,95	4000	5,33	0,26	32,00	2.12	5.24	0.09	23.83	2.63
5	1,13	4000	6,40	0,21	27,80	4.28	4.88	0.02	23.69	2.78
6	1,65	4000	6,71	0,29	28,00	2.36	6.42	0.12	18.13	1.25
7	2,57	10,000	5,75	0,69	17,12	4.17	6.86	0.15	11.15	3.14
8	3,28	10,000	7,95	0,11	11,09	1.01	8.78	0.16	9.37	1.19
9	3,58	10,000	9,46	0,11	9,07	0.04	11.54	0.01	5.86	0.1
10	5,55	5000	19,13	2,52	26,55	11.55	11.81	0.99	43.05	13.43

Note: P_{max} is the value of the maximum loading, E is the modulus of elasticity, R_w is the damage index, E_{10} is the modulus of elasticity measured at tenth cycle of cyclic nanoindentation, R_{w10} is the damage index measured at the tenth cycle of cyclic nanoindentation, StDev is the standard deviation of the indicated values

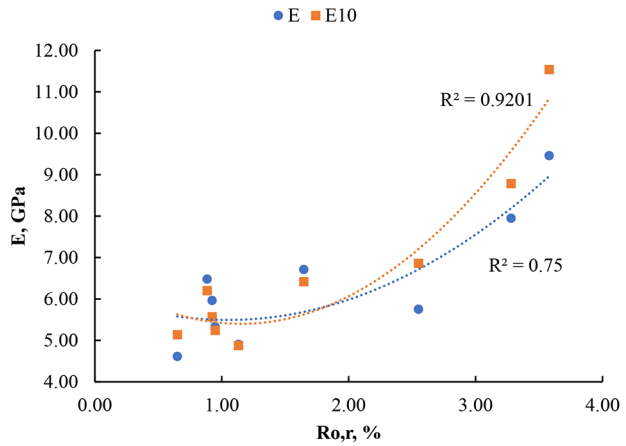

Fig. 5 Correlations between coal rank and values of the elastic moduli

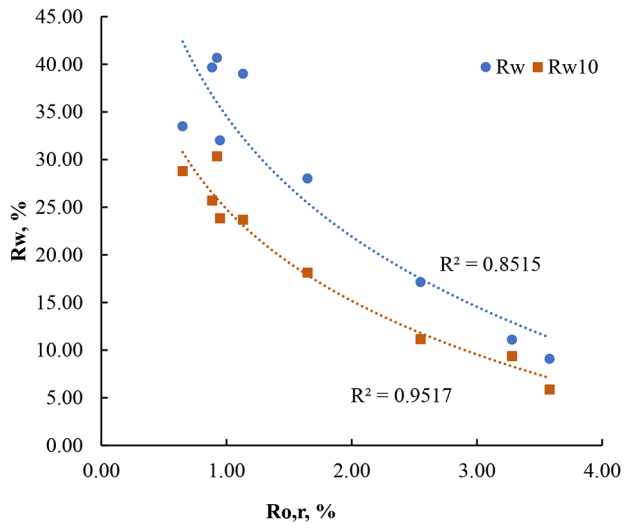

Fig. 6 Correlations between coals vitrinite reflectance and their ability to crushing (damage indices)

Table 5 Alteration of coals mechanical properties during cyclic nanoindentation

Sample No.	$E_{compaction}$ (%)	$R_{compaction}$ (%)
1	-11.41	14.03
2	4.29	35.20
3	6.61	25.37
4	1.65	25.53
5	0.49	39.26
6	4.38	35.26
7	-19.27	34.90
8	-10.52	15.52
9	-22.01	35.40
10	38.29	-62.16

Quantification of coals mechanical properties alteration at cyclic mechanical impacts was carried out by calculating the following parameters $E_{compaction}$, $R_{compaction}$:

$$E_{compaction} = \frac{E - E_{10}}{E} \times 100\%, \quad (1)$$

$$R_{compaction} = \frac{R_w - R_{w10}}{R_w} \times 100\%. \quad (2)$$

The calculated parameters are listed in Table 5.

The negative values of $E_{compaction}$ parameter refer to the fact that elastic modulus of coal matter after ten sequential nanoindentation tests is higher than that measured by quasi-static nanoindentation. I.e., a 'compaction' phenomenon is observed.

Consideration of data shown in Table 5; Fig. 3 allowed the following observations.

For coals of the first group, $E_{compaction}$ are mostly negative or close to zero (with the exception of coal No. 2 of the Pechora basin). The $R_{compaction}$ values of this group are the highest, mostly 35% and over.

Table 6 Fitting parameters of coals "D" and "G" bands on basis of raw Raman spectra

Sample No.	*X* D	*X* G	*I* D	*I* G	*A* D	*A* G	FWHM D	FWHM G
1	1348	1583	172	186	45,387	20,227	248.13	102.32
2	1346	1582	267	286	63,385	31,304	222.62	102.89
3	1347	1578	360	365	72,468	42,996	189.25	110.71
4	1346	1576	115	108	20,946	13,345	170.71	116.22
5	1344	1582	108	108	26,389	11,624	228.97	101.30
6	1342	1583	107	103	26,329	11,320	231.55	103.64
7	1328	1591	145	274	26,641	37,835	172.77	129.88
8	1326	1591	158	265	26,826	37,938	159.32	134.47
9	1323	1583	1061	957	285,157	96,747	252.55	94.98
10	1343	1587	705	495	114,486	49,335	61.67	24.61

Note: *X* means the exact position of the corresponding peak (1/cm), *I* means intensity, *A* means area, FWHM means full width half maximum

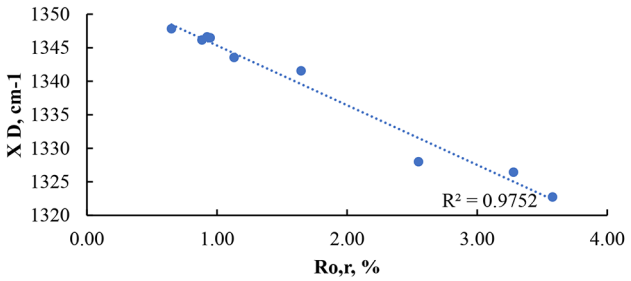

Fig. 7 Correlation between the "D" band peak location and coals vitrinite reflectance index

For coals of the second group, the $E_{compaction}$ parameters are also negative, and $R_{compaction}$ is less than 35% for both coals.

For coals of the third group in terms of the character of the change in mechanical properties during cyclic indentation, the $E_{compaction}$ parameter is positive. The $R_{compaction}$ parameter is similar to the coals of the 2nd group.

3.2 Raman spectroscopy study of coal structure

Table 6 contains the results of the measured parameters of wide "D" and "G" bands of the coals and graphite Raman spectra.

As it has been previously mentioned by (Ulyanova et al. 2014), there is almost no correlation between the parameters of the wide "D" and "G" bands of coals with their rank with the exception of the location of the highest point of "D" peak based on the raw Raman data. In our research, we have obtained similar correlation shown in Fig. 7. The only exception was the natural graphite No. 10, presumably, due to its different structure.

One of the semi-quantitative parameters of raw Raman data that is in relation with coals mechanical properties is the ratio of "D" to "G" peaks areas demonstrating the 'disordered' to 'graphitic' structures shares in coals, as shown in Fig. 8.

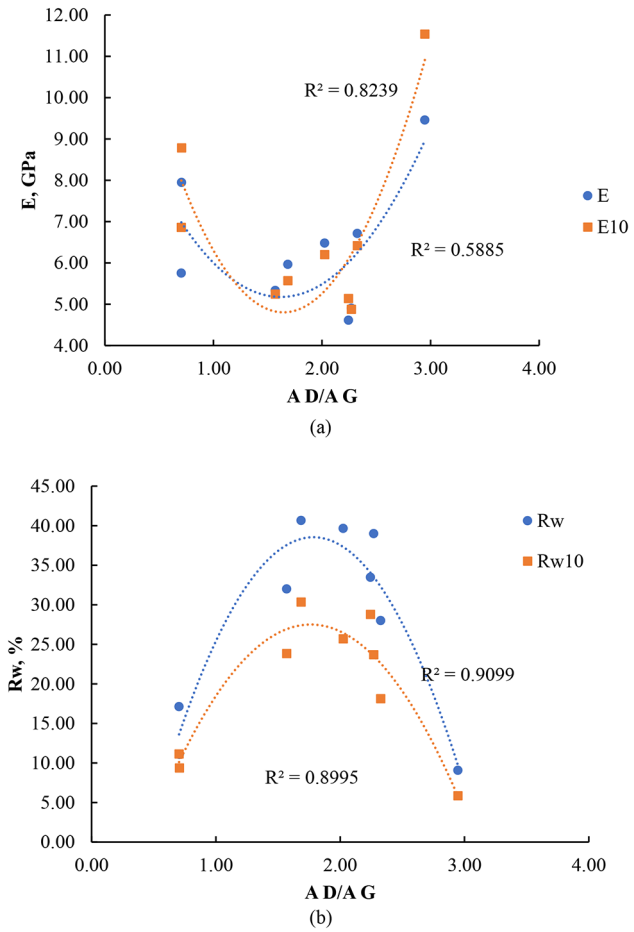

Fig. 8 Correlations between coals mechanical properties for **a** Elastic moduli **b** Damage index, and some structural parameters measured by Raman spectroscopy

The correlations shown in Fig. 8 are the U-shaped dependency of coals mechanical properties and propensity to destruction on the share of 'disordered' to 'graphitic' structures in organic matter. It was found that anthracite No. 9 (Donetsk coal basin) is at the end of one branch (on the right) at both the graphs, whereas metaanthracite No. 8 and anthracite No. 7 (Omsukchansk coal field) are located at the

Table 7 Raman spectra peaks fitting data

Sample No.	SL		D		VR		VL		GR		G		G2	
	X (1/cm)	*A*	*X* (1/cm)	*A*	*X* (1/cm)	*A*	*X* (1/cm)	*A*	*X* (1/cm)	*A*	*X* (1/cm)	*A*	*X* (1/cm)	*A*
1	1274	14,330	1350	29,601			1442	9912	1548	8823	1582	9040	1609	6487
2	1252	22,184	1331	30,250	1371	7657	1433	22,044	1551	12,922	1583	13,023	1609	10,277
3	1234	18,502	1311	29,069	1362	32,098	1440	20,267	1551	15,448	1582	17,364	1609	13,565
4	1239	4159	1322	10,172	1368	13,364	1482	4120	1560	4711	1587	4550	1611	3460
5	1247	8008	1324	12,117	1369	7435	1434	2515	1507	3212	1571	7470	1604	5169
6	1245	8887	1325	11,237	1368	6674	1431	3782	1512	3415	1573	6599	1604	5065
7	1236	6987	1331	20,369	1368	1501			1568	12,266	1589	13,042	1607	9549
8	1248	11,735	1326	12,778	1368	6041			1551	6476	1585	15,989	1605	13,719
9	1213	67,212	1324	223,566	1365	51,127			1509	45,088	1575	55,109	1600	44,995
10			1344	141,590							1580	30,807	1606	24,462

Note: *X* is the Raman shift of the peak maximum, *A* is fitted peak area

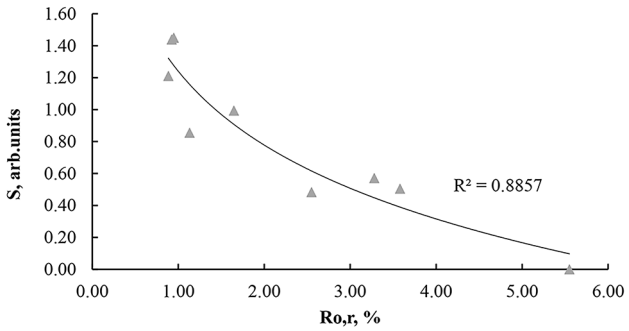

Fig. 9 Relation between the ratio of amorphous to crystalline carbon in coals with vitrinite reflectance

end of the left branch. Therefore, it could be concluded that interpretation of the raw Raman spectral data (namely, the wide "D" and "G" bands consideration) is not enough for characterization of features and nature of coals destruction modes under the mechanical impacts.

The results of more detailed consideration of the Raman spectral data (namely, peaks identification and fitting in accordance with Table 2) are shown in Table 7. It could be noted that according to graphite No. 10 spectral data deconvolution, peaks D, G and G2 are related to crystalline carbon, and are present in its structure, whereas all the others that were found only in coals, are related to carbon in its amorphous form. The sum of areas of peaks assigned to the amorphous carbon ($S_{\text{amorphous}}$) was calculated:

$$S_{\text{amorphous}} = \text{ASL} + \text{AVR} + \text{AVL} + \text{AGR} \tag{3}$$

as well as for the peaks assigned to crystalline form of carbon (S_{crystal}):

$$S_{\text{crystal}} = \text{AD} + \text{AG} + \text{AG2} \tag{4}$$

Further, the share of amorphous carbon in crystalline one was calculated as

$$S = \frac{S_{\text{amorphous}}}{S_{\text{crystal}}} \tag{5}$$

The correlation between the parameter *S* and vitrinite reflection indices was found as shown in Fig. 9. It reveals an exponential decay of vitrinite reflectance with increase of amorphous carbon share to its crystalline form.

It is well known that increase of crystalline carbon in coals with rank is primarily associated with increase of number and sizes of graphitic (aromatic) layers and their re-orientation from disordered to well aligned with respect to the bedding direction along with decrease of the interlayer spacing (Hirsch 1954; Zhang et al. 2021). Along with it, the amorphous carbon is related to non-aromatic carbon compounds such as hydrocarbons, OH-groups, methyl and methylene groups, 2–4 rings aromatics with defects, etc. (Hirsch 1954; Bodzek and Marzec 1981; Marzec 2000, 2002). Amorphous carbon is being found in high-rank coals such as anthracites and metaanthracites and vanishes only at the stage of natural graphite, as it has been previously shown in by XRD analysis (Li et al. 2021). Amorphous carbon primarily plays a role of crosslinks between aromatic clusters, but their bonding energy is smaller than the bonding energy within the graphitic quasi-crystals (clusters) (Hirsch 1954; Marzec 1986). The latter determines the 'liquid structure' of middle-rank coals that are able to melt at relatively low temperatures during the coking process (Hirsch 1954). Destruction of the crosslinks between the clusters by sorption treatment with dimethylformamide leads to decrease of hardness of coals by two times and more (Epshtein et al. 2007). Therefore, it could be assumed that at mechanical loading, the primary zones of defects initiation and formation could be associated with the zones of more weak intermolecular bonding, namely, the amorphous carbon structures (crosslinks).

As it is shown in Fig. 10, the damage index of coals (excluding graphite) also correlates (for both static R_w and cyclic R_{w10}) with the share of amorphous carbon with respect

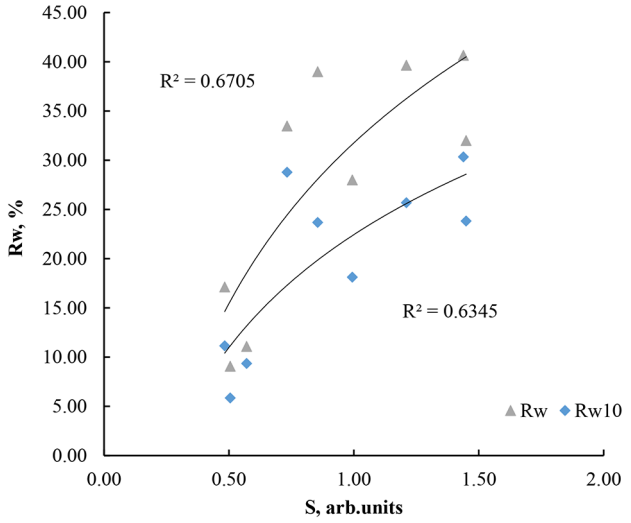

Fig. 10 Relation between damage indices of coals and graphite on the share of amorphous carbon with respect to crystallite one

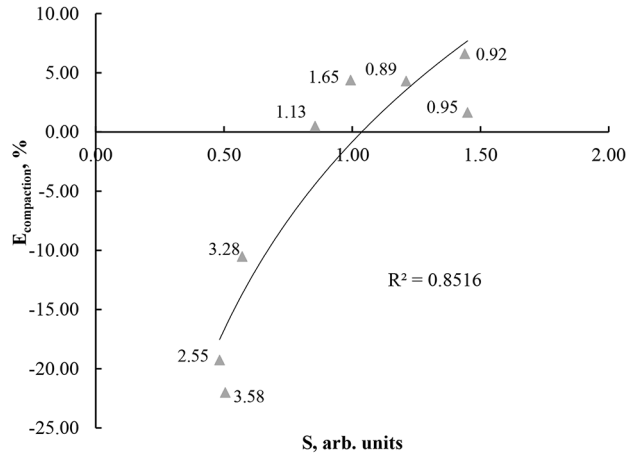

Fig. 11 Correlation of the degree of coal matter compaction during cyclic nanoindentation with amorphous carbon share. Numbers near the dots denote vitrinite reflectance index $R_{o,r}$ of the corresponding coal

to crystallite one. This allows to conclude that the growth of amorphous carbon contents in coals generally leads to increase of their propensity to crushing under mechanical effects.

The degree of changing of coals elastic moduli after the cyclic nanoindentation with respect to statically measured, i.e. $E_{compaction}$ (Eq. (1)) also well correlates with the share of amorphous carbon. This is illustrated in Fig. 11 (excluding graphite No. 10). Thus, the parameter $E_{compaction}$ could be considered as a degree of fine particles compaction (including the previously formed fine particles) during cyclic loading of coals. The smaller this value is, the larger the degree of compaction. Here, we should consider the real values of $E_{compaction}$, not by modulo.

Data shown in Fig. 11 reveals that the degree of coals matter compaction at cyclic nanoindentation after ten cycles increases with the decrease of S ratio. Therefore, it could be assumed that when the ratio of amorphous to crystalline carbon in coals reaches 1 and exceeds this value, coals matter becomes rather brittle and tends to bulk crushing during relatively surface-based mechanical effects such as cyclic nanoindentation. It is worth mentioning that in general, the mechanism of coals' destruction (on the basis of $E_{compaction}$ parameter) depends on the amorphous to crystalline carbon share S. Preliminarily, it has been shown that anthracites of different origins and metaanthracite are characterized by local crushing within the contact area with the indenter.

Some basic characteristics that were obtained for characterization of coals fine structure from Raman spectra deconvolution could be of help to preliminary predict coals propensity to crushing and fine dust formation during external mechanical impacts. This characteristic is the ratio between amorphous and crystalline carbon in coals. If it exceeds 1, then these coals are more prone to bulk destruction. If it is less than 1, then the coal matter crushing becomes local but is presumably being accompanied with fine dust release during mechanical impacts.

4 Conclusions

Based on analysis of results of cyclic nanoindentation with increasing peak load, the studied coals were divided into three groups. Each of the groups included coals of different rank. Coals assigned to the first two groups are characterized by local crushing in the zone of contact with the indenter tip. The mode of their destruction is similar and differs only in the degree of alteration of elastic moduli and damage indices from cycle to cycle. Coals of the third group are prone to bulk crushing, i.e. both in the contact zone and outside it.

For high-rank coals (with vitrhinte reflectance index of 2% and higher), the stiffness of the coal substance (modulus of elasticity) increases with the rank.

Parameters R_w proportionally descend with coals rank growth. Damage indices measured after the tenth cycle of nanoindentation for all the studied coals are lower than those determined by the quasi-static nanoindentation method. This is due to the destruction of the coal matter under cyclic loading with formation of fine powder (dust particles) and the compaction of it in the subsequent cycles.

New parameter $E_{compaction}$ was introduced for quantification of coals mechanical properties changes under cyclic mechanical loading. It denotes the degree of coals matter compaction or bulk destruction within the selected mode of loading.

The ratio between the amorphous and crystalline phases of carbon (S) was calculated by deconvolution of coals Raman spectra. It is established that this parameter is in the functional dependency with the value of the vitrinite reflection index.

The susceptibility of coals to destruction (damage index) increases with an increase of the amorphous carbon in the coal matter. Moreover, high contents of amorphous carbon are one of the reasons of bulk destruction of coals matter under cyclic mechanical effects. On the other hand, when S parameter is lower than 1, the coals are being crushed only in the zone of contact with the indenter.

Acknowledgements The research was financially supported by the Russian Science Foundation grant (#18-77-10052).

Author Contributions EK and SE contributed to the study conception and design. Data collection and analysis were performed by EK and SE. Samples preparation and petrographic analysis were performed by VK and JH. Nanoindentation experiments, results collection and evaluation were done by MM. Raman spectroscopy experiments were done by JH and VK. The first draft of the manuscript was written by EK. All authors have commented on previous versions of the manuscript. All authors read and approved the final manuscript.

Funding The research was funded by the Russian Science Foundation grant (#18-77-10052).

Data Availability All data generated or analyzed during this study are included in this published paper.

Declarations

Competing interests The authors have no competing interests to declare that are relevant to the content of this article.

References

Aneja VP, Isherwood A, Morgan P (2012) Characterization of particulate matter (PM 10) related to surface coal mining operations in Appalachia. Atmos Environ 54:496–501. https://doi.org/10.1016/j.atmosenv.2012.02.063

Argatov II, Borodich FM, Epshtein SA, Kossovich EL (2017) Contact stiffness depth-sensing indentation: understanding of material properties of thin films attached to substrates. Mech Mater 114:172–179. https://doi.org/10.1016/j.mechmat.2017.08.009

Baafi EY, Ramani RV (1979) Rank and maceral effects on coal dust generation. Int J Rock Mech Min Sci Geomech Abstr 16:107–115. https://doi.org/10.1016/0148-9062(79)91447-5

Barsoum MW, Murugaiah A, Kalidindi SR et al (2004) Kink bands, nonlinear elasticity and nanoindentations in graphite. Carbon N Y 42:1435–1445. https://doi.org/10.1016/j.carbon.2003.12.090

Baruya P (2012) Losses in the coal supply chain

Beron AI, Pozin EZ, Melamed VZ (1971) Distribution pattern of the grain-size composition of coal fractured by cutting. Sov Min Sci 7:512–517. https://doi.org/10.1007/BF02501061

Bodzek D, Marzec A (1981) Molecular components of coal and coal structure. Fuel 60:47–51. https://doi.org/10.1016/0016-2361(81)90030-2

Bulychev SI, Alekhin VP, Shorshorov MK et al (1975) Determination of Young modulus by the hardness indentation diagram. Zavod Lab 41:1137–1140

Epshtein SA, Barabanova OV, Minaev VI et al (2007) Effect of dimethylformamide treatment of coals on their thermal degradation and elastic-plastic properties. Solid Fuel Chem 41:210–215. https://doi.org/10.3103/S0361521907040052

Epshtein SA, Kossovich EL, Prosina VA, Dobryakova NN (2018) Features of sorption-induced strength degradation of coals originated from potentially prone to outburst and non-hazardous packs. Gorn Zhurnal 18–22. https://doi.org/10.17580/gzh.2018.12.04

Epshtein SA, Kossovich EL, Vishnevskaya EP et al (2020) Determination of total and fine airborne dust in coals. Min informational Anal Bull 5–14. https://doi.org/10.25018/0236-1493-2020-6-0-5-14

Erol I, Aydin H, Didari V, Ural S (2013) Pneumoconiosis and quartz content of respirable dusts in the coal mines in Zonguldak, Turkey. Int J Coal Geol 116–117:26–35. https://doi.org/10.1016/j.coal.2013.05.008

Fender TD, Rouainia M, Van Der Land C et al (2020) Geomechanical properties of coal macerals; measurements applicable to modelling swelling of coal seams during CO2 sequestration. Int J Coal Geol 228:103528. https://doi.org/10.1016/j.coal.2020.103528

Han Y, Wang J, Dong Y et al (2017) The role of structure defects in the deformation of anthracite and their influence on the macromolecular structure. Fuel 206:1–9. https://doi.org/10.1016/j.fuel.2017.05.085

Hirsch PB (1954) X-Ray scattering from coals. Proc R Soc A Math Phys Eng Sci 226:143–169. https://doi.org/10.1098/rspa.1954.0245

Hower JC, Graese AM, Klapheke JG (1987) Influence of microlithotype composition on hardgrove grindability for selected eastern Kentucky coals. Int J Coal Geol 7:227–244. https://doi.org/10.1016/0166-5162(87)90038-3

Huan X, Tang YG, Xu JJ et al (2019) Structural characterization of graphenic material prepared from anthracites of different characteristics: A comparative analysis. Fuel Process Technol 183:8–18. https://doi.org/10.1016/j.fuproc.2018.08.017

Jiang J, Zhang S, Longhurst P et al (2021) Molecular structure characterization of bituminous coal in Northern China via XRD, Raman and FTIR spectroscopy. Spectrochim Acta Part A Mol Biomol Spectrosc 255:119724. https://doi.org/10.1016/j.saa.2021.119724

Kossovich EL, Dobryakova NN, Epshtein SA, Belov DS (2016) Mechanical properties of coal microcomponents under continuous indentation. J Min Sci 52:906–912. https://doi.org/10.1134/S1062739116041382

Kossovich EL, Borodich FM, Epshtein SA, Galanov BA (2020a) Indentation of bituminous coals: fracture, crushing and dust formation. Mech Mater 150:103570. https://doi.org/10.1016/j.mechmat.2020.103570

Kossovich EL, Epshtein SA, Dobryakova NN, Minin MG (2020b) Structural features and mechanical properties of anthracite,

metaanthracite and graphite. Gorn Zhurnal 2020:25–29. https://doi.org/10.17580/gzh.2020.04.05

Kossovich EL, Epshtein SA, Golubeva MD, Krasilova VA (2021) On using cyclic nanoindentation technique to assess coals propensity to fine dust formation. Min informational Anal Bull 112–121. https://doi.org/10.25018/0236_1493_2021_5_0_112

Li K, Liu Q, Cheng H et al (2021) Classification and carbon structural transformation from anthracite to natural coaly graphite by XRD, Raman spectroscopy, and HRTEM. Spectrochim Acta - Part A Mol Biomol Spectrosc 249:119286. https://doi.org/10.1016/j.saa.2020.119286

Liu T, Liu S (2020) The impacts of coal dust on miners' health: a review. Environ Res 190:109849. https://doi.org/10.1016/j.envres.2020.109849

Luo Y, Wang D, Cheng J (2017) Effects of rock dusting in preventing and reducing intensity of coal mine explosions. Int J Coal Sci Technol 4:102–109. https://doi.org/10.1007/s40789-017-0168-z

Manoj B (2016) A comprehensive analysis of various structural parameters of indian coals with the aid of advanced analytical tools. Int J Coal Sci Technol 3:123–132. https://doi.org/10.1007/s40789-016-0134-1

Marzec A (1986) Macromolecular and Molecular Model. Fuel Process Technol 14:39–46

Marzec A (2000) Intermolecular interactions of aromatic hydrocarbons in carbonaceous materials a molecular and quantum mechanics. Carbon N Y 38:1863–1871

Marzec A (2002) Towards an understanding of the coal structure: a review. Fuel Process Technol 77–78:25–32. https://doi.org/10.1016/S0378-3820(02)00045-0

Moreno T, Trechera P, Querol X et al (2019) Trace element fractionation between PM10 and PM2.5 in coal mine dust: implications for occupational respiratory health. Int J Coal Geol 203:52–59. https://doi.org/10.1016/j.coal.2019.01.006

Nikitin AP, Khabibulina ER, Mikhaylova ES et al (2019) Structural defects and the demineralization of Kuznetsk Basin coal: data from Raman Spectroscopy. Coke Chem 62:169–173. https://doi.org/10.3103/S1068364X19050028

Organiscak JA, Page SJ (1993) Laboratory investigation of coal grindability and airborne respirable dust. J Mine Vent Soc South Africa 46:98–105

Organiscak JA, Page SJ (2000) Airborne Dust Liberation during Coal Crushing. Coal Prep 21:423–453. https://doi.org/10.1080/07349340108945630

Pandey B, Agrawal M, Singh S (2016) Ecological risk assessment of soil contamination by trace elements around coal mining area. J Soils Sediments 16:159–168. https://doi.org/10.1007/s11368-015-1173-8

Panov GE (1967) Dust formation kinetics as a function of the principal mechanical properties of coals. Sov Min Sci 3:511–514. https://doi.org/10.1007/BF02497948

Sadezky A, Muckenhuber H, Grothe H et al (2005) Raman microspectroscopy of soot and related carbonaceous materials: spectral analysis and structural information. Carbon N Y 43:1731–1742. https://doi.org/10.1016/j.carbon.2005.02.018

Shekarian Y, Rahimi E, Shekarian N et al (2021) An analysis of contributing mining factors in coal workers' pneumoconiosis prevalence in the United States coal mines, 1986–2018. Int J Coal Sci Technol 8:1227–1237. https://doi.org/10.1007/s40789-021-00464-y

Si L, Cao Y, Fan G, Wang S (2020) Study on fracture shape distribution characteristics and micromechanical properties of middling coal. AIP Adv 10:075324. https://doi.org/10.1063/5.0015946

Ul'yanova EV, Malinnikova ON, Pashichev BN, Malinnikova EV (2019) Microstructure of coal before and after gas-dynamic phenomena. J Min Sci 55:701–707. https://doi.org/10.1134/S1062739119056063

Ulyanova EV, Molchanov AN, Prokhorov IY, Grinyov VG (2014) Fine structure of Raman spectra in coals of different rank. Int J Coal Geol 121:37–43. https://doi.org/10.1016/j.coal.2013.10.014

Vasilenko T, Islamov A, Kirillov A et al (2020) Investigation of Tectonically Disturbed Zones of coal seams of the Kuznetsk Coal Basin using SANS. J Surf Investig X-ray. Synchrotron Neutron Tech 14:S235–S241. https://doi.org/10.1134/S1027451020070496

Vranjes S, Misch D, Schöberl T et al (2018) Nanoindentation study of macerals in coals from the ukrainian Donets Basin. Adv Geosci 45:73–83. https://doi.org/10.5194/adgeo-45-73-2018

Xu RT, Li HJ, Hou QL et al (2015) The effect of different deformation mechanisms on the chemical structure of anthracite coals. Sci China Earth Sci 58:502–509. https://doi.org/10.1007/s11430-014-4998-x

Xu J, Tang H, Su S et al (2018) A study of the relationships between coal structures and combustion characteristics: the insights from micro-raman spectroscopy based on 32 kinds of chinese coals. Appl Energy 212:46–56. https://doi.org/10.1016/j.apenergy.2017.11.094

Zhang Y, Lebedev M, Al-Yaseri A et al (2018) Nanoscale rock mechanical property changes in heterogeneous coal after water adsorption. Fuel 218:23–32. https://doi.org/10.1016/j.fuel.2018.01.006

Zhang Y, Lebedev M, Smith G et al (2020) Nano-mechanical Properties and Pore-Scale characterization of different rank coals. Nat Resour Res 29:1787–1800. https://doi.org/10.1007/s11053-019-09572-8

Zhang X, Wang S, Chen H et al (2021) Aromatic structural characterization of different-rank vitrinites: using HRTEM, XRD and AFM. Polycycl Aromat Compd 41:1319–1330. https://doi.org/10.1080/10406638.2019.1676267

Zhou W, Wang H, Wang D et al (2019) The effect of coal proximate compositions on the characteristics of dust generation using a conical pick cutting system. Powder Technol 355:573–581. https://doi.org/10.1016/j.powtec.2019.07.093